Acta Crystallographica Section D
Biological Crystallography
ISSN 0907-4449

Structural analysis of *Pneumocystis carinii* and human DHFR complexes with NADPH and a series of five potent 6-[5′-(ω-carboxyalkoxy)benzyl]-pyrido[2,3-*d*]pyrimidine derivatives

Vivian Cody[a,b]* and Jim Pace[a]

[a]Structural Biology Department, Hauptman–Woodward Medical Research Institute, 700 Ellicott Street, Buffalo, New York 14203, USA, and [b]Structural Biology Department, School of Medicine and Biological Sciences, State University of New York at Buffalo, USA

Correspondence e-mail: cody@hwi.buffalo.edu

Received 13 August 2010
Accepted 12 October 2010

PDB References: pcDHFR–**1**, 3nz6; pcDHFR–**2**, 3nz9; pcDHFR–**3**, 3nza; pcDHFR–**4**, 3nzb; pcDHFR–**5**, 3nzc; hDHFR–**3**, 3nzd.

Structural data are reported for five antifolates, namely 2,4-diamino-6-[5′-(5-carboxypentyloxy)-2′-methoxybenzyl]-5-methylpyrido[2,3-*d*]pyrimidine, (**1**), and the 5′-[3-(ethoxycarbonyl)propoxy]-, (**2**), 5′-[3-(ethoxycarbonyl)butoxy]-, (**3**), 5′-[3-(ethoxycarbonyl)pentyloxy]-, (**4**), and 5′-benzyloxy-, (**5**), derivatives, which are potent and selective for *Pneumocystis carinii* dihydrofolate reductase (pcDHFR). Crystal structures are reported for their ternary complexes with NADPH and pcDHFR refined to between 1.4 and 2.0 Å resolution and for that of **3** with human DHFR (hDHFR) to 1.8 Å resolution. These data reveal that the carboxylate of the ω-carboxyalkoxy side chain of **1**, the most potent inhibitor in this series, forms ionic interactions with the conserved Arg75 in the substrate-binding pocket of pcDHFR, whereas the less potent ethyl esters of **2**–**4** bind with variable side-chain conformations. The benzyloxy side chain of **5** makes no contact with Arg75 and is the least active inhibitor in this series. These structural results suggest that the weaker binding of this series compared with that of their pyrimidine homologs in part arises from the flexibility observed in their side-chain conformations, which do not optimize intermolecular contact to Arg75. Structural data for the binding of **3** to both hDHFR and pcDHFR reveals that the inhibitor binds in two different conformations, one similar to each of the two conformations observed for the parent pyrido[2,3-*d*]pyrimidine, piritrexim (PTX), bound to hDHFR. The structure of the pcDHFR complex of **4** reveals disorder in the side-chain orientation; one orientation has the ω-carboxyalkoxy side chain positioned in the folate-binding pocket similar to the others in this series, while the second orientation occupies a new site near the nicotinamide ring of NADPH. This alternate binding site has not been observed in other DHFR structures. Structural data for the pcDHFR complex of **5** show that its benzyl side chain forms intermolecular van der Waals interactions with Phe69 in the binding pocket that could account for its enhanced binding selectivity compared with the other analogs in this series.

1. Introduction

Opportunistic infections by *Pneumocystis* pathogens are still a leading cause of mortality and morbidity among patients with AIDS or other immunosuppressed conditions (Thomas & Limper, 2004). The primary treatment for *Pneumocystis* pneumonia (PcP) combines a sulfonamide drug with trimethoprim (TMP; Fig. 1), which targets the folate pathway. TMP has been widely used as an antibiotic as it is a highly selective competitive inhibitor of bacterial dihydrofolate

Table 1
Enzyme inhibition against DHFR for selected inhibitors (Fig. 1; Chan *et al.*, 2005; Rosowsky *et al.*, 2004).

Inhibitor	IC_{50}, pcDHFR (n*M*)	IC_{50}, rat DHFR (n*M*)	Rat DHFR/pcDHFR selectivity ratio
TMP	13000	180000	13.8
PTX	13	3.3	0.26
PY957	0.049	3.9	80
PY1011	1.0	5000	5000
1	1.3	2.0	1.5
2	6.5	4.2	0.65
3	28	14	0.50
4	35	21	0.60
5	96	170	1.8

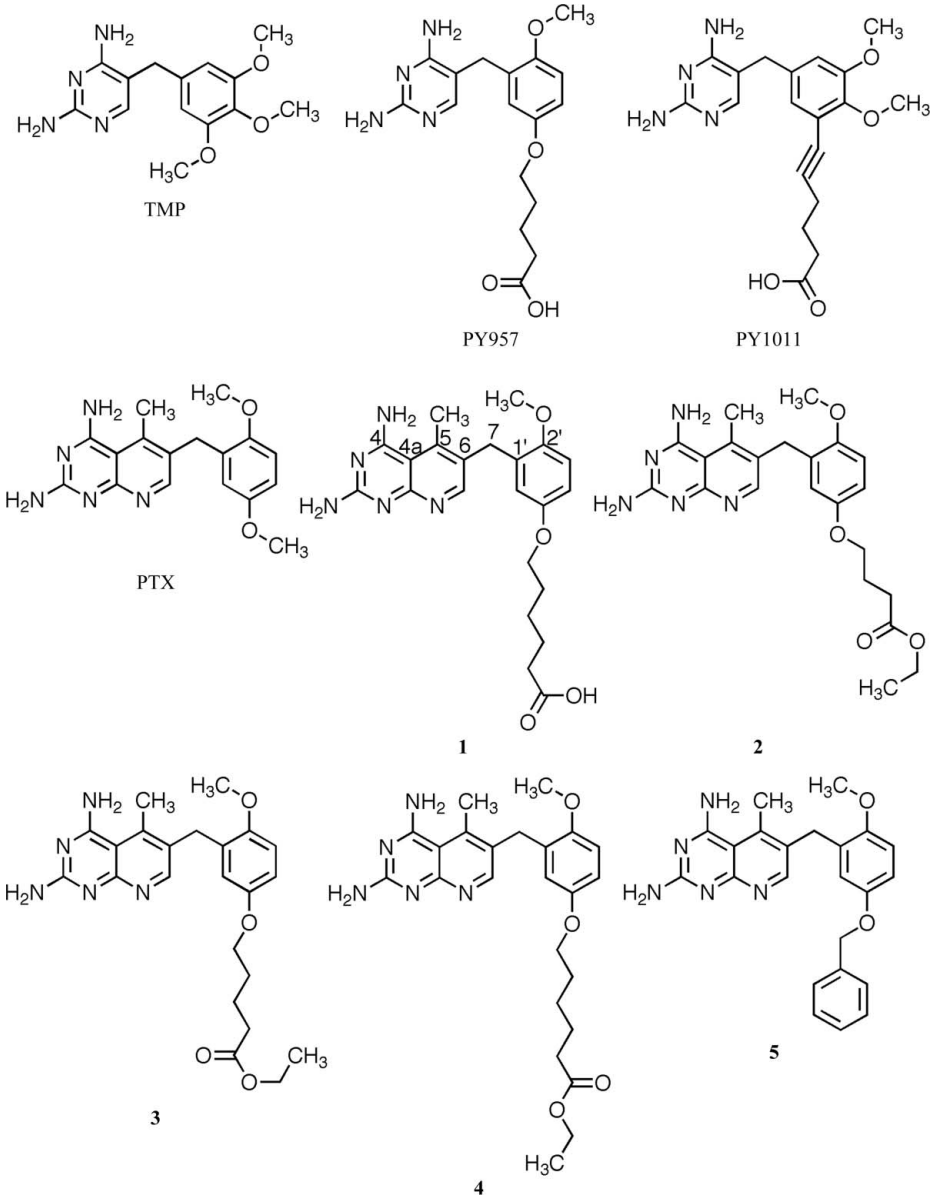

Figure 1
Schematic representation of the antifolates under study. 2,4-diamino-6-[5′-(5-carboxypentyloxy)-2′-methoxybenzyl]-5-methylpyrido[2,3-*d*]pyrimidine, (1); 2,4-diamino-6-{5-[3-(ethoxycarbonyl)propoxy]-2-methoxybenzyl}-5-methylpyrido[2,3-*d*]pyrimidine, (2); 2,4-diamino-6-{5-[3-(ethoxycarbonyl)butoxy]-2-methoxybenzyl}-5-methylpyrido[2,3-*d*]pyrimidine, (3); 2,4-diamino-6-{5-[3-(ethoxycarbonyl)pentyloxy]-2-methoxybenzyl}-5-methylpyrido[2,3-*d*]pyrimidine, (4); and 2,4-diamino-6-(5-benzyloxy-2-methoxybenzyl)-5-methylpyrido[2,3-*d*]pyrimidine, (5).

reductase (DHFR) and is currently used in the treatment of PcP (Rosowsky *et al.*, 2003), although its use in combination therapy with a sulfonamide that targets the dihydropteroate pathway is not always successful. TMP has limited efficacy in PcP patients and can result in drug resistance (Nahimana *et al.*, 2004). Therefore, there is still a need to develop more effective treatments.

As part of a larger program to design lipophilic DHFR inhibitors that would contain structural features of both piritrexim (PTX) and TMP (Fig. 1), used in the treatment of *Pneumocystis* pneumonia (PcP), Rosowsky and coworkers have synthesized a number of compounds that incorporate the 2′,5′-dimethoxybenzyl substitution pattern of PTX with the diaminopyrimidine-5-(3′,4′,5′-trimethoxybenzyl) pattern of TMP (Chan *et al.*, 2005; Rosowsky *et al.*, 2004). To further define inhibitor classes that combine the high potency of PTX with the high antiparasitic *versus* mammalian selectivity of TMP, a similar series of *ω*-carboxyalkoxypyrido[2,3-*d*]pyrimidines, both as carboxylates and their ethyl esters, were designed and tested (Chan *et al.*, 2005). These data revealed that the ester derivatives were less potent than the carboxylate parent compounds as measured by their IC_{50} values using recombinant protein (Table 1).

Activity data for the series of diaminopyrimidines that have the TMP template revealed that the optimal length of the *ω*-carboxyalkoxy side chain was for the carboxybutyloxybenzyl side chain of PY957 and the carboxy-1-pentyloxybenzyl side chain of PY1011 (Fig. 1), which had selectivity ratios of 80 and 5000, respectively, for rat DHFR/pcDHFR IC_{50} (Rosowsky *et al.*, 2004; Table 1). The sequence of rat DHFR has 89% identity and 96% similarity to that of human DHFR. None of the differences involve active-site residues. Structural data for PY1011 and PY957 revealed that the inhibitor carboxylate forms a strong salt bridge to the conserved Arg75 in the pcDHFR active site, similar to that observed for the folate substrate or methotrexate inhibitor complexes (Cody *et al.*, 1999, 2006). In this series of

Table 2
Crystal properties and refinement statistics for inhibitors **1**–**5** bound to pcDHFR and hDHFR as NADPH ternary complexes.

Values in parentheses are for the highest resolution shells.

	pcDHFR–**1**	pcDHFR–**2**	pcDHFR–**3**	pcDHFR–**4**	pcDHFR–**5**	hDHFR–**3**
PDB code	3nz6	3nz9	3nza	3nzb	3nzc	3nzd
Space group	$P2_1$	$P2_1$	$P2_1$	$P2_1$	$P2_1$	$H3$
Unit-cell parameters						
a (Å)	37.1	36.9	36.9	36.9	36.9	84.6
b (Å)	42.8	42.7	42.7	42.7	42.7	84.6
c (Å)	60.8	60.1	60.6	60.6	59.9	77.6
β (°)	94.4	94.8	94.6	94.6	94.8	
Beamline	SSRL 11-1	SSRL 11-1	SSRL 11-1	SSRL 11-1	SSRL 11-1	SSRL 9-2
Resolution	1.80 (1.86–1.80)	1.60 (1.66–1.60)	1.70 (1.76–1.70)	1.30 (1.37–1.30)	1.80 (1.86–1.80)	1.80 (1.90–1.80)
Wavelength (Å)	0.975	0.975	0.975	0.975	0.975	0.975
$R_{\rm merge}$	0.070 (0.58)	0.028 (0.33)	0.070 (0.38)	0.046 (0.46)	0.060 (0.34)	0.062 (0.34)
Completeness (%)	96.3 (98.8)	96.6 (90.3)	97.8 (98.0)	87.5 (47.3)	95.8 (83.8)	95.3 (74.2)
Observed reflections	17172	46806	21070	154924	17462	67454
Unique reflections	12344	24011	19449	44341	16720	18315
$\langle I/\sigma(I)\rangle$	14.4 (0.58)	13.1 (5.0)	14.4 (4.4)	12.8 (1.7)	4.9 (0.5)	15.0 (3.3)
Multiplicity	3.7 (1.2)	3.6 (3.2)	2.5 (2.0)	3.4 (2.1)	3.5 (3.0)	3.7 (3.2)
Resolution range	32.7–2.0 (2.1–2.0)	24.5–1.6 (1.7–1.6)	27.8–1.8 (1.9–1.8)	24.7–1.4 (1.5–1.4)	32.5–1.9 (2.0–1.9)	53.3–1.8 (1.9–1.8)
Reflections used	11724	16107	13884	30117	11845	17366
R factor	0.21	0.20	0.21	0.24	0.21	0.16
$R_{\rm free}$	0.28	0.27	0.28	0.29	0.27	0.23
Total protein/ligand atoms	1931	1879	1893	1892	1782	1878
Total waters	166	114	116	73	48	296
Average B factor (Å^2)	32.0	30.0	29.3	25.4	41.3	19.6
Error in Luzzati plot	0.29	0.21	0.23	0.21	0.25	0.17
R.m.s. deviation from ideal						
Bond lengths (Å)	0.019	0.023	0.022	0.022	0.022	0.025
Bond angles (°)	2.11	2.34	2.00	2.02	1.98	2.23
Ramachandran plot (%)						
Most favored	91.2	94.6	92.1	93.6	89.2	96.7
Additional	5.4	3.4	4.0	3.9	7.8	2.7
Disallowed	3.4	1.5	4.0	2.5	2.9	0.5
Missing density†	1–4, 83–89	1, 4, 83–89	1–4, 83–89	1–4, 83–89	1–4, 83–89	

† Residues without interpretable density and not refined.

pyrido[2,3-*d*]pyrimidines selectivity was uniformly reduced, with the most selective of these five inhibitors being **1**, which contains a 5′-carboxybutyloxybenzyl side chain (Fig. 1). Compound **3** also has a butyloxybenzyl side chain but is an ethyl ester and has a selectivity ratio about half that of compound **1** (Table 1).

In order to validate the binding mode of these pyrido[2,3-*d*] pyrimidines, we report structural data for ternary complexes of pcDHFR with NADPH and a series of five ω-carboxyalkoxy inhibitors (Fig. 1) that explore the effects of side-chain length and ester formation on pcDHFR binding. Additionally, the crystal structure of **3** is reported as a ternary complex with human DHFR (hDHFR).

2. Methods

2.1. Crystallization and X-ray data collection

Recombinant pcDHFR was cloned, expressed and purified as described previously (Delves *et al.*, 1993). The protein was washed in a Centricon-10 three times with 10 m*M* MES buffer pH 6.0, 100 m*M* KCl and concentrated to 15.5–21.7 mg ml^{-1} pcDHFR for the five complexes. The protein was incubated with the antifolates (**1**–**5**; Fig. 1) and NADPH prior to crystallization using the hanging-drop vapor-diffusion method at 277 K. The protein droplets for the pcDHFR complexes contained 33–36% PEG 2K, 46–52 m*M* MES pH 6 with 100 m*M* KCl. Cryogenic solutions for the pcDHFR crystals were prepared using mother liquor with a 16–24% gradient of ethylene glycol.

Recombinant hDHFR was expressed in pDS5 vector in *Escherichia coli* BL21 (DE3) cells and purified as described previously (Cody *et al.*, 2009). The protein was concentrated to 6.9 mg ml^{-1} and incubated with **3** and NADPH prior to crystallization using the hanging-drop vapor-diffusion method at 287 K. The protein droplets contained 100 m*M* potassium phosphate pH 6.9 and 30% ammonium sulfate. The reservoir consisted of 100 m*M* potassium phosphate pH 6.9, 65% ammonium sulfate and 3%(*v*/*v*) ethanol. The hDHFR complex crystal was cryoprotected with Paratone-N oil (Hampton Research, Aliso Viejo, California, USA).

Data for the pcDHFR and hDHFR inhibitor complexes were collected to 1.4–2.0 Å resolution on beamlines 11-1 or 9-2 at the Stanford Synchrotron Resource Laboratory (SSRL) using the remote-access protocol (McPhillips *et al.*, 2002; Cohen *et al.*, 2002; González *et al.*, 2008). All data were processed in *HKL*-2000 using *DENZO* and were scaled with *SCALA* (Otwinowski & Minor, 1997). The unit-cell parameters and diffraction statistics for these ternary complexes are listed in Table 2.

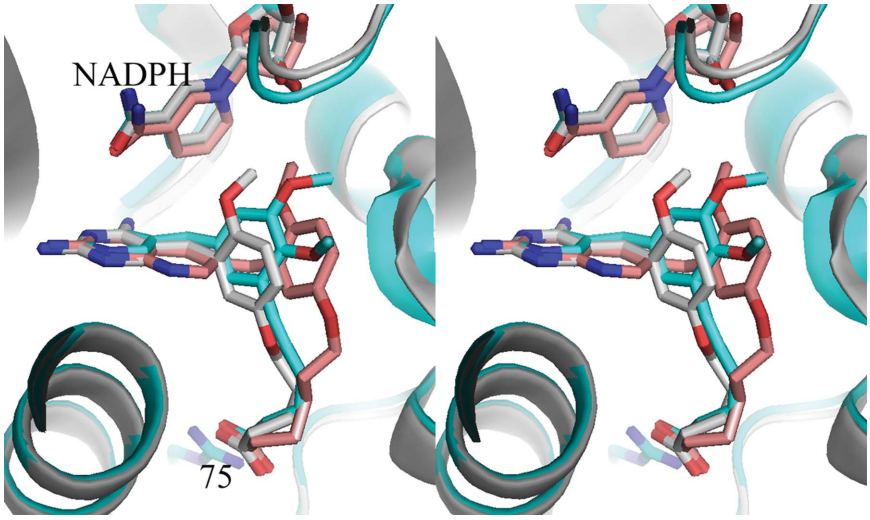

Figure 2
Stereo superposition of **1** (pink) with PY957 (grey) and PY1011 (cyan) in the structures of their ternary complexes with pcDHFR and NADPH (Cody *et al.*, 2006). The active-site residue Arg75 is shown.

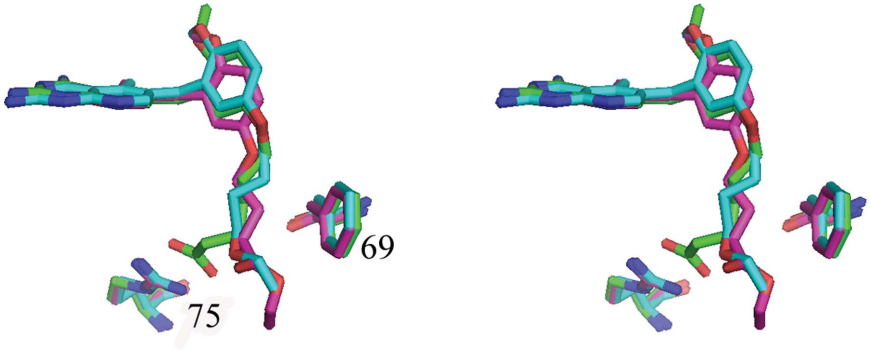

Figure 3
Stereo superposition of inhibitors **1** (green), **2** (cyan) and **3** (violet) in their ternary complexes with pcDHFR and NADPH. The active-site residues Arg75 and Phe69 are shown.

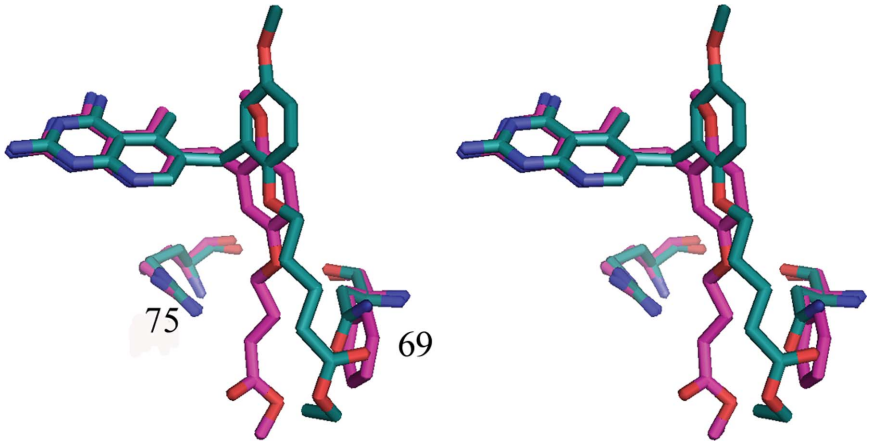

Figure 4
Comparison of the binding of **3** in the pcDHFR–NADPH ternary complex (violet) and the hDHFR–NADPH ternary complex (blue). Also shown are residues Arg75 and Phe69 in pcDHFR and Arg70 and Asn64 in hDHFR.

2.2. Structure determination and refinement

All structures were solved by molecular-replacement methods with *MOLREP* (Vagin & Teplyakov, 2010; Collaborative Computational Project, Number 4, 1994) using the coordinates for pcDHFR (PDB entry 3cd2; Cody *et al.*, 1999) and hDHFR (PDB entry 1u72; Cody *et al.*, 2005). Inspection of the resulting difference electron-density maps was made using the program *Coot* (Emsley & Cowtan, 2004) running on a Mac G5 workstation and revealed density for ternary complexes in all cases. To monitor the refinement, a random subset of all reflections was set aside for calculation of $R_{\rm free}$ (5%). The models for the antifolates were generated from the crystal structure of PY957 (Cody *et al.*, 2006) and optimized with *SYBYL* (Tripos). The parameter files for the cofactor and inhibitors were prepared using the Dundee *PRODRG*2 server website (http://davapc1.bioch.dundee.ac.uk/programs/prodrg; Schüttelkopf & van Aalten, 2004). Refinement was carried out using the program *REFMAC*5 from the *CCP*4 suite of programs (Collaborative Computational Project, Number 4, 1994). Between least-squares minimizations, the structures were manually adjusted to fit difference electron density. The Ramachandran conformational parameters generated by *RAMPAGE* (Lovell *et al.*, 2002) for the final models from the last cycle of refinement are listed in Table 2. Coordinates for these structures have been deposited in the Protein Data Bank and their PDB codes are listed in Table 2. Superimpositions were computed using the same structure as reference molecule with the SSM function in *Coot*. Figures were prepared using the modeling program *PyMOL* (DeLano, 2006).

3. Results

Inspection of the difference electron-density maps for pcDHFR with the five pyrido[2,3-*d*]pyrimidine inhibitors (**1**–**5**; Fig. 1) revealed ternary complexes with NADPH in all cases. The lack of clearly interpretable electron density for loop 83–89 in each of these pcDHFR complexes indicates that this region is highly mobile and represents alternate conformational states compared with the structures previously reported in

Table 3
Conformational parameters for methylene bridge of pyrimidine and pyrido[2,3-*d*]pyrimidine inhibitors (Fig. 1).

The torsion angles used are defined in **1** (Fig. 1).

	C5—C6—C7—C1′ (°)	C6—C7—C1′—C2′ (°)	C4—C4a—C5 (°)
pcDHFR–**1**	153.4	−93.9	123.8
pcDHFR–**2**	151.7	−95.7	125.6
pcDHFR–**3**	169.2	−96.0	124.8
pcDHFR–**4**	−148.2	−114.3	126.3
pcDHFR–**4**	−174.2	85.4	126.3
pcDHFR–**5**	174.8	−94.1	129.1
pcDHFR–PY957†	179.0	91.0	—
pcDHFR–PY1011†	177.2	74.1	—
hDHFR–**3**	115.6	105.7	125.3
hDHFR-L22R–PTX‡	145.1	−89.5	127.0
hDHFR–PTX‡	123.5	108.8	129.9

† Cody *et al.* (2006). ‡ Lewis *et al.* (1995).

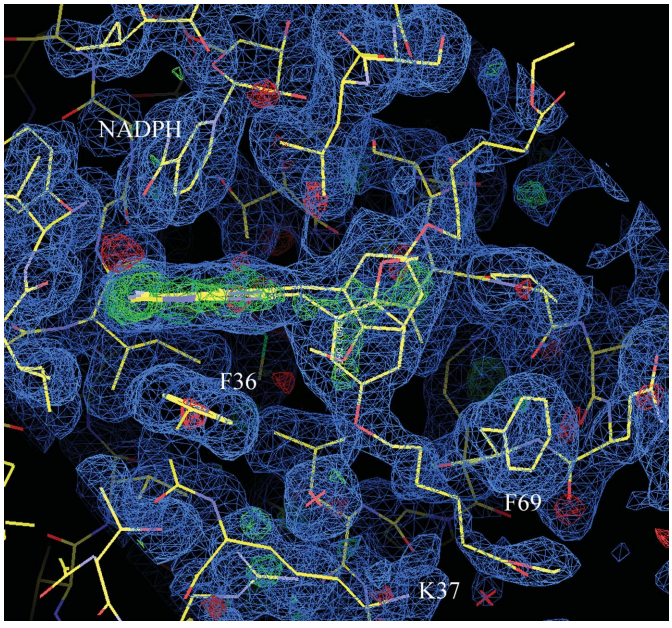

Figure 5
View of the $2F_o - F_c$ difference electron-density map (0.5σ, blue) showing two conformations for **4**, each refined at half occupancy, in the ternary complex with pcDHFR and NADPH. The green density, contoured at 3σ, is from an $F_o - F_c$ OMIT map calculated without contributions from **4**. Key residues in the active site are labeled for orientation.

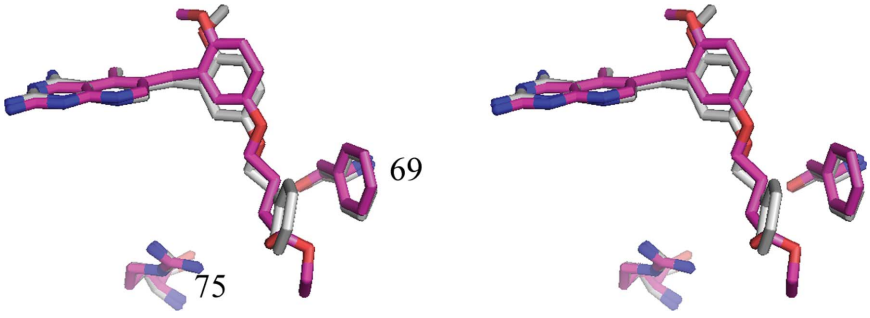

Figure 6
Stereo superposition of the binding of **5** (grey) with that of **3** (violet), highlighting the hydrophobic interactions of the benzyl ether with Phe69, in the ternary complexes with pcDHFR and NADPH.

other pcDHFR complexes (Cody *et al.*, 1999; Cody & Schwalbe, 2006). Similarly, there was poor electron density for the first four N-terminal residues. These residues were not included in the refinement.

As previously described (Cody *et al.*, 2005, 2006; Cody & Schwalbe, 2006), the side chain of the conserved Arg75 in pcDHFR is held in place by a network of hydrogen bonds to the conserved Thr38 and Thr39 and the backbone functional groups of Lys68 and, through water, to the backbone carbonyl of Phe69. There are also *cis*-peptide linkages between Arg67 and Pro68 and Gly124 and Gly125, as observed in other pcDHFR complexes. The interactions of the 2,4-diamino-pyrido[2,3-*d*]pyrimidine ring of these antifolates preserve the overall pattern of contacts with invariant residues in the active site. The hydrogen-bond network involving structural water, the conserved residues Thr144, Trp27 and Glu32 and the N1 nitrogen and 2-amino group of the pyrido[2,3-*d*]pyrimidine ring is also maintained. Similarly, the inhibitor 4-amino group maintains its contacts with the conserved residues Ile9 and Tyr129 and NADPH. In all these structures, the cofactor NADPH is bound in an extended conformation similar to other pcDHFR or hDHFR cofactor complexes (Cody & Schwalbe, 2006).

The pyrido[2,3-*d*]pyrimidine inhibitor **3** is the ethyl ester homologue of the potent TMP analogue PY957 (Fig. 1), as both inhibitors have a 5′-carboxybutyl side chain. In this series of pyrido[2,3-*d*]pyrimidines, only inhibitor **1**, which has a carboxypentyloxybenzyl side chain, is a carboxylate analogue similar to the potent pyrimidine analogs reported previously (Rosowsky *et al.*, 2004). Structural data for the binding of inhibitor **1** to pcDHFR reveal that despite the difference in size of the pyrimidine ring of the TMP template *versus* that of the pyrido[2,3-*d*]pyrimidine ring, the 5′-carboxypentyloxy-benzyl side chain of **1** adjusts its conformation to form a salt bridge with Arg75 similar to that observed for the potent inhibitors PY957 and PY1011 (Cody *et al.*, 2006) (Fig. 2). Torsion angles that describe the bridging geometry between ring systems, defined in **1** (Fig. 1), reveal that the conformation of these inhibitors is similar (Table 3). In the case of inhibitor **3**, the ethyl ester homologue of PY957, the side chain moves away from Arg75, similar to that of inhibitor **2** (Fig. 3).

Structural data for inhibitor **2**, which has the shortest side chain (5′-carbethoxypropyloxybenzyl), shows that its conformation is similar to that of **1**; however, there is limited interaction with Arg75 as the ethyl ester forces the side chain to move away from Arg75. Similar interactions were observed for the ternary complex of pcDHFR with **3**, which has a 5′-carbethoxybutyloxybenzyl side chain (Fig. 3). Analysis of the structure of the hDHFR ternary complex with **3** reveals that the conformation of the inhibitor differs from that observed in the pcDHFR complex (Fig. 4), as is shown by the bridging torsion angles (Table 3). In the hDHFR complex the ethyl ester carbonyl forms a strong

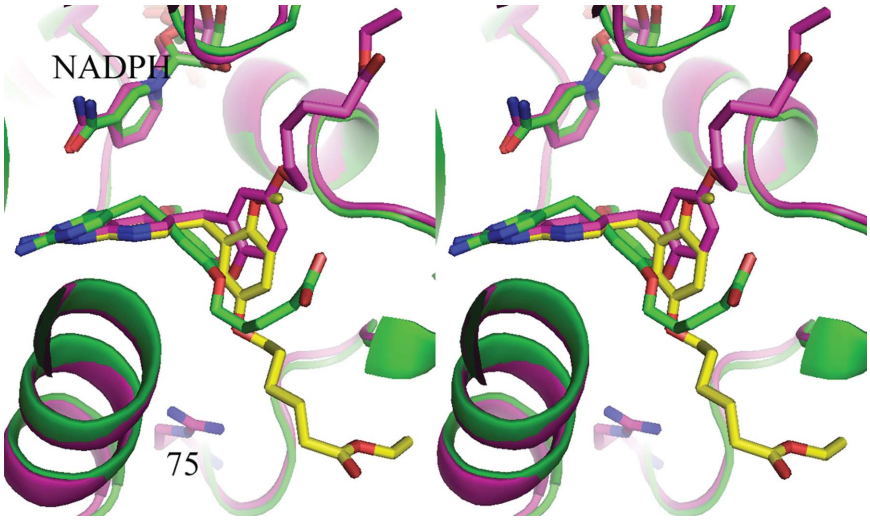

Figure 7
Stereoview of the binding modes of the two alternate conformations of **4** (yellow and violet) in the structure of the pcDHFR–NADPH ternary complex (violet) compared with that of PY957 in the Q35S/N64F double mutant of hDHFR (green). The position of the conserved Arg75 that normally binds the carboxylate of the inhibitor is shown.

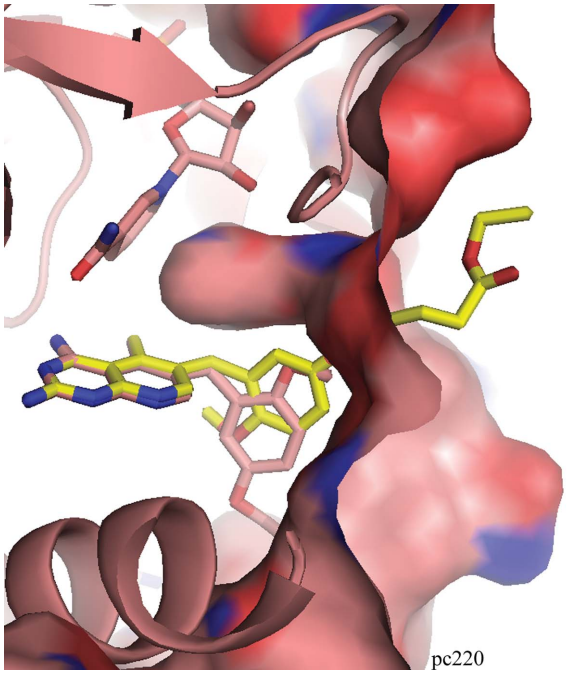

Figure 8
van der Waals surface of the ternary complex of pcDHFR with **4** and NADPH showing the positions of the two alternate conformations of **4** (yellow and pink). The surface profile for pcDHFR shows a pocket that extends toward the nicotinamide ribose ring of NADPH that is not present in hDHFR (surface not shown).

hydrogen bond contact (2.8 Å) to the amine of the Asn64 side chain. In the pcDHFR complex the corresponding residue is Phe69, which forms close van der Waals contacts to the methylene C atoms of the inhibitor side chain.

Of the five structures determined for this series, **4** is the most interesting in that analysis of the difference electron-density map shows that the 5-carbethoxypentyloxybenzyl side chain occupies two positions: one conformer is bound in the same way as the other inhibitors in this series, while the second conformer occupies a position observed for the first time binding in a pocket near NADPH (Fig. 5). Based on the electron-density profile, each side chain was refined with 50% occupancy.

Inhibitor **5** has a 2′-*O*-benzyl ether side chain and therefore is not able to interact with Arg75; however, there are good hydrophobic contacts between the benzyl side chain of **5** and Phe69 that enhance the binding to pcDHFR (Fig. 6).

4. Discussion

This structural study of a series of *O*-(*ω*-carboxyalkoxy) analogs of PTX (**1**–**5**; Fig. 1) that have variable length side chains with and without ethyl esters revealed that the carboxybutyl carboxylate side chain of **1** was optimal for interaction with the conserved Arg75 in the active site of pcDHFR. The presence of the ethyl ester causes the side chain to move away from Arg75 to make hydrophobic interactions with Phe69 in the pcDHFR active site. The replacement of Phe69 by Asn64 in hDHFR results in a conformational change in the binding of **3** compared with that to pcDHFR as the carbonyl of the side chain of **3** forms a hydrogen bond to Asn64 (Fig. 4). In addition, there is a conformational change in the bridging torsion angle of **3** between the two structures (Table 3). These changes are consistent with the greater potency of **3** for mammalian DHFR compared with pcDHFR (Table 1).

The most unexpected results were observed for inhibitor **4**, which showed that the carbethoxypentyloxybenzyl side chain binds in two alternate conformations, one of which is near the nicotinamide ring of NADPH, a region not previously occupied by a ligand. The position of the second conformer of **4** also differs significantly from the other examples of alternative binding conformers observed in the crystal structure of PY957 bound to the Q35S/N64F double mutant of hDHFR (Cody *et al.*, 2009; Fig. 7). Examination of this region of pcDHFR reveals the presence of a pocket below the nicotinamide ring that is open to the surface (Fig. 8). However, this pocket is not present in the hDHFR structure. These differences suggest that changes in the surface profile of the DHFR can influence the binding environment and could be of importance in understanding structure–activity profiles for ligand-binding efficacy.

Analysis of the DHFR binding of the parent pyrido[2,3-*d*]pyrimidine PTX also revealed that alternate conformers were observed for its binding to hDHFR (Lewis *et al.*, 1995; Cody & Schwalbe, 2006). Comparison of these PTX structures with the carboxyalkyoxy pyrido[2,3-*d*]pyrimidine analogs reported here shows a clustering of the conformers observed for these structures. The conformation of **3** in hDHFR is

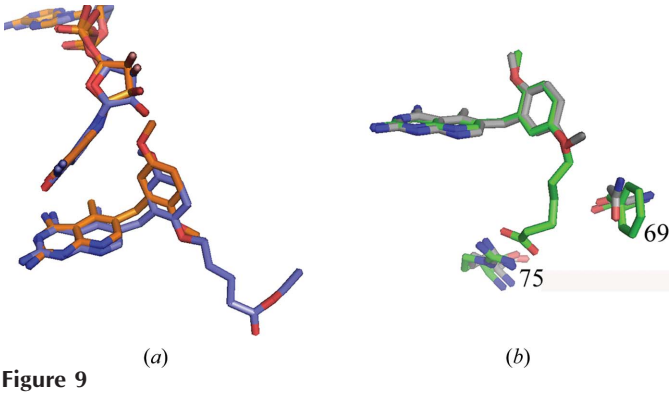

Figure 9
Comparison of the binding of PTX in hDHFR–NADPH (gold) (*a*) with **3** (blue) in pcDHFR and (*b*) with **1** (green) and PTX (grey) in the L22R mutant of hDHFR (Lewis *et al.*, 1995). Conformational angles about the methylene bridge for these inhibitors are shown in Table 3.

similar to that observed for PTX in wild-type hDHFR, while that of **1** in pcDHFR is similar to that of PTX in the L22R mutant of hDHFR (Table 3; Fig. 9). The crystal structure of PTX in complex with pcDHFR has been reported previously (Champness *et al.*, 1994); however, no coordinates are available and thus no comparisons could be made with the structures of the hDHFR–PTX complexes. Taken together, these structural results suggest that the clustering observed for the conformational parameters of PTX and the pyrido[2,3-*d*]pyrimidine analogs **1**–**5**, although small, could be the result of subtle changes in the interactions of specific residues in the active site with the ligand. Therefore, these patterns could be of importance when computing preferential binding geometries in homology models.

In summary, these data show that the pyrido[2,3-*d*]pyrimidine *O*-(*ω*-carboxyalkoxybenzyl) scaffold of this series of DHFR inhibitors results in weaker potency and selectivity compared with the homologous analogs in the pyrimidine series (Chan *et al.*, 2005; Rosowsky *et al.*, 2004; Table 1). Structural data for the variable-length acids and esters of the carbalkyoxybenzyl analogs shows that the ethyl esters are not able to optimize the binding interactions within the *p*-aminobenzyoylglutamate binding pocket and that their side-chain orientations were highly variable among the analogs studied. This variability in binding that does not utilize strong interactions with the conserved Arg75 observed for folate analogs is consistent with the weaker binding observed for this series.

This work was supported in part by grant GM51670 from the National Institutes of Health (VC). The authors thank Dr Andre Rosowsky for supplying the antifolates for study, Kim Chisum for crystal-growth experiments, Dr Edward Snell for his help in data collection and processing and the beamline staff at SSRL for their support. Portions of this research were carried out at the Stanford Synchrotron Radiation Laboratory, a national user facility operated by Stanford University on behalf of the US Department of Energy, Office of Basic Energy Sciences. The SSRL Structural Molecular Biology Program is supported by the Department of Energy, Office of Biological and Environmental Research and by the National Institutes of Health, National Center for Research Resources, Biomedical Technology Program and the National Institute of General Medical Sciences.

References

Champness, J. N., Achari, A., Ballantine, S. P., Bryant, P. K. & Stammers, D. K. (1994). *Structure*, **2**, 915–924.
Chan, D. C., Fu, H., Forsch, R. A., Queener, S. F. & Rosowsky, A. (2005). *J. Med. Chem.* **48**, 4420–4431.
Cody, V., Galitsky, N., Rak, D., Luft, J. R., Pangborn, W. & Queener, S. F. (1999). *Biochemistry*, **38**, 4303–4312.
Cody, V., Luft, J. R. & Pangborn, W. (2005). *Acta Cryst.* D**61**, 147–155.
Cody, V., Pace, J., Chisum, K. & Rosowsky, A. (2006). *Proteins*, **65**, 959–969.
Cody, V., Pace, J., Makin, J., Piraino, J., Queener, S. F. & Rosowsky, A. (2009). *Biochemistry*, **48**, 1702–1711.
Cody, V. & Schwalbe, C. H. (2006). *Crystallogr. Rev.* **12**, 301–333.
Cohen, A. E., Ellis, P. J., Miller, M. D., Deacon, A. M. & Phizackerley, R. P. (2002). *J. Appl. Cryst.* **35**, 720–726.
Collaborative Computational Project, Number 4 (1994). *Acta Cryst.* D**50**, 760–763.
DeLano, W. L. (2006). *PyMOL.* http://www.pymol.org.
Delves, C. J., Ballantine, S. P., Tansik, R. L., Baccanari, D. P. & Stammers, D. K. (1993). *Protein Expr. Purif.* **4**, 16–23.
Emsley, P. & Cowtan, K. (2004). *Acta Cryst.* D**60**, 2126–2132.
González, A., Moorhead, P., McPhillips, S. E., Song, J., Sharp, K., Taylor, J. R., Adams, P. D., Sauter, N. K. & Soltis, S. M. (2008). *J. Appl. Cryst.* **41**, 176–184.
Lewis, W. S., Cody, V., Galitsky, N., Luft, J. R., Pangborn, W., Chunduru, S. K., Spencer, H. T., Appleman, J. R. & Blakley, R. L. (1995). *J. Biol. Chem.* **270**, 5057–5064.
Lovell, S. C., Davis, I. W., Arendell, W. B. III, de Baker, P. I. W., Word, J. M., Prisant, M. G., Richardson, J. S. & Richardson, D. C. (2002). *Proteins*, **50**, 437–450.
McPhillips, T. M., McPhillips, S. E., Chiu, H.-J., Cohen, A. E., Deacon, A. M., Ellis, P. J., Garman, E., Gonzalez, A., Sauter, N. K., Phizackerley, R. P., Soltis, S. M. & Kuhn, P. (2002). *J. Synchrotron Rad.* **9**, 401–406.
Nahimana, A., Rabodonirina, M., Bille, J., Francioli, P. & Hauser, P. M. (2004). *Antimicrob. Agents Chemother.* **48**, 4301–4305.
Otwinowski, Z. & Minor, W. (1997). *Methods Enzymol.* **276**, 307–326.
Rosowsky, A., Forsch, R. A. & Queener, S. F. (2003). *J. Med. Chem.* **46**, 1726–1736.
Rosowsky, A., Fu, H., Chan, D. C. & Queener, S. F. (2004). *J. Med. Chem.* **47**, 2475–2485.
Schüttelkopf, A. W. & van Aalten, D. M. F. (2004). *Acta Cryst.* D**60**, 1355–1363.
Thomas, C. F. & Limper, A. H. (2004). *N. Engl. J. Med.* **350**, 487–2498.
Vagin, A. & Teplyakov, A. (2010). *Acta Cryst.* D**66**, 22–25.